Rev. Adv. Mater. Sci. 28 (2011) 74-78

MICROSTRUCTURES AND ELECTROCHEMICAL PROPERTIES OF RAPIDLY-SOLIDIFIED Si-Mn ALLOY

Hyun Wook Han[1], Deuk Kyu Ahn[1], Hyo-Jun Ahn[2], Won-Wook Park[1] and Keun Yong Sohn[1]

[1]School of Nano Engineering, Inje University, 607 Obang-dong, Gimhae, Gyeongnam 621-749, Republic of Korea
[2]School of Nano and Advanced Materials Engineering, Gyeongsang National University, 900 Gazwa-dong, Chinju, Gyeongnam 660-701, Republic of Korea

Received: February 17, 2011

Abstract. The microstructure and electrochemical properties of a $Si_{70}Mn_{30}$ alloy prepared by melt spinning and arc melting have been investigated. Melt-spun ribbons and arc-melted ingots were fragmented and mixed with acetylene black (AB), polyvinylidene fluoride (PVDF), and *N*-methylpyrrolidinone by planetary milling for 2 h to characterize their electrochemical properties. The results showed that the microstructures of the melt-spun ribbons represented a fine eutectic constituent composed of a silicon phase with a thickness of approximately 50~70 nm and a Mn_4Si_7 compound. The cyclic behavior of the rapidly solidified melt-spun $Si_{70}Mn_{30}$ ribbons improved remarkably over that of the arc-melted specimens because of a finer microstructural scale; as the thickness of silicon crystal decreased 40 fold, the initial irreversible capacity was reduced by more than 2.5 times. The improved cycle performance of the melt-spun ribbons is a consequence of the small diffusion distance for the lithium-ion exchange.

1. INTRODUCTION

Lithium-ion batteries are known to be the best commercial rechargeable batteries because of their high specific capacity and excellent cycle life. Enhancing their energy density has been an issue during the last decade. Graphitic or graphitization carbons have been used extensively as negative electrode materials for lithium-ion batteries. The theoretical capacity of graphite is 372 $mAhg^{-1}$ [1-2]. Silicon is an attractive anode material because of its high intercalation capacity [3]. However, silicon-based anode materials show a poor cycle life owing to large variations in the volume of the silicon particles [4]. The cycle performance of Si-based anode materials improves with decreasing size of silicon particles [5]. Si-Mn binary alloys show the capability to be used as materials for a secondary battery. The second discharge capacity of a $Si_{70}Mn_{30}$ sputtered alloy by atomic ratio was reported to be approximately 1000 $mAhg^{-1}$ [5].

In order to effectively improve the cycle performance, fine silicon particles should be dispersed in the conducting host matrix. In this work, $Si_{70}Mn_{30}$ binary alloys by atomic ratio were prepared by melt spinning and arc melting. Since their chemical composition is close to the eutectic point and melt spinning is a rapid solidification process, the melt-spun alloy ribbons are expected to have a fine eutectic constituent. The objectives of this work are to identify the phases in the rapidly solidified Si-Mn ribbons and their relative effects on the electrochemical behavior of the material, and to investigate the effect of the microstructural scale on the electrochemical properties of the $Si_{70}Mn_{30}$ near-eutectic alloy.

Corresponding author: Keun Yong Sohn, e-mail: ksohn@inje.ac.kr

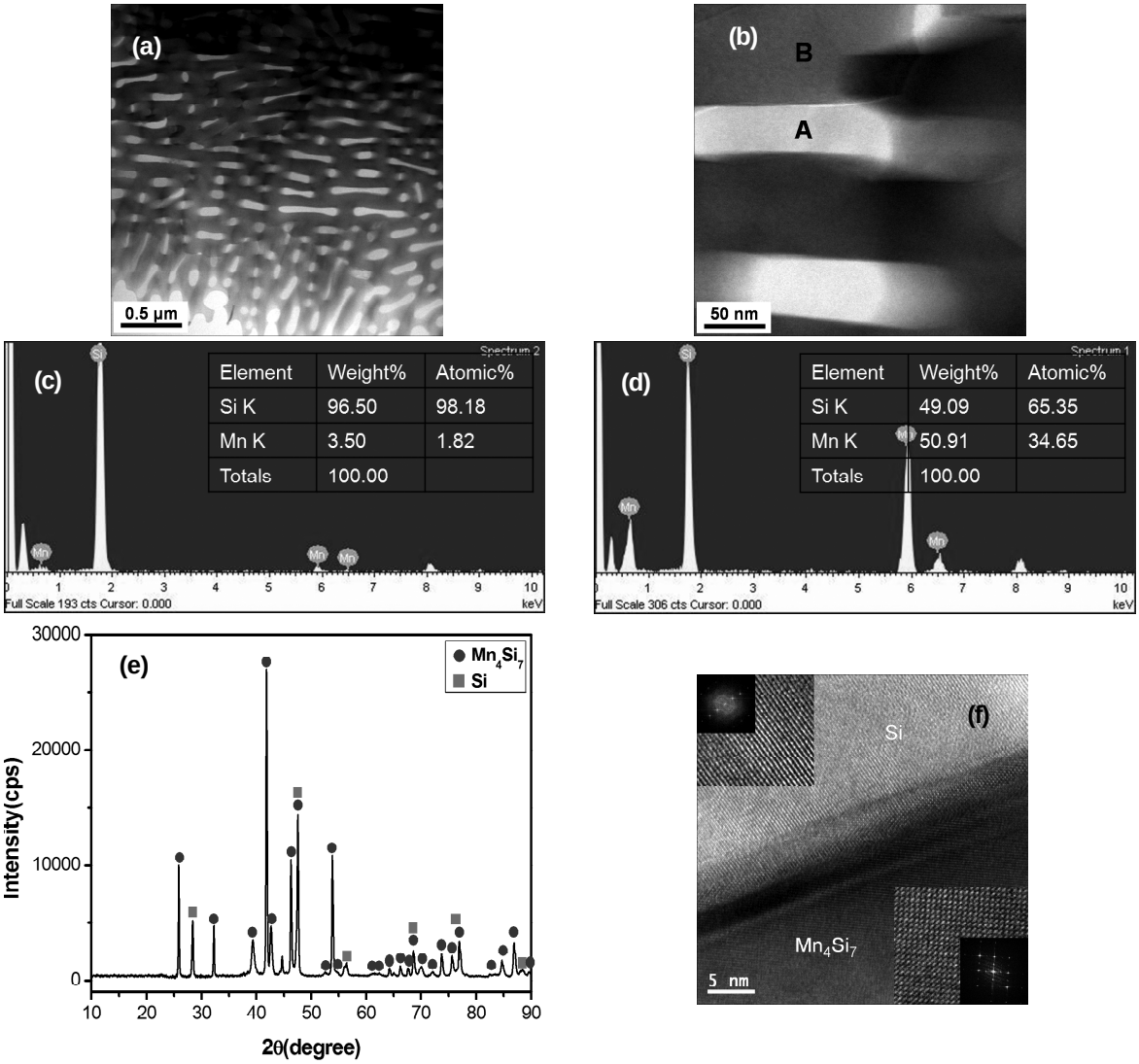

Fig. 1. Microstructures and X-ray diffraction patterns of melt-spun $Si_{70}Mn_{30}$ ribbons: (a) BFTEM; (b) Enlarged view of (a); (c) EDS of Area A of (b); (d) EDS of Area B of (b); (e) X-ray diffraction patterns; (f) HRTEM of area (b).

2. EXPERIMENTAL PROCEDURE

Si-30at.%Mn alloy specimens used in this study were prepared from high-purity silicon (99.999%) and commercial-grade pure manganese (99.8%) by two different processes: arc melting and arc melting followed by melt spinning. Conventionally solidified specimens were prepared by arc melting under an argon atmosphere to produce button-shaped ingots weighing ~5 g. In order to prepare rapidly solidified ribbons, the raw materials were prealloyed by arc melting under an argon atmosphere. The prealloyed ingots were melt spun to produce the rapidly solidified ribbons, for which the ingots were induction melted in a cylindrical graphite tube and ejected through a small orifice 0.3 mm in diameter using argon gas at a pressure of 0.4 kgf/cm^2. The ejected liquid jet impinged on a copper wheel rotating at 2,200 rpm to produce ~1 mm-wide and 20 μm-thick ribbons.

The ribbons and arc-melted ingots were fragmented by mortar milling to produce a powder that could be passed through a 270-mesh sieve. Subsequently, acetylene black (AB), polyvinylidene fluoride (PVDF), and *N*-methylpyrrolidinone (NMP, 5 cc) were added into the alloy powder and mixed by planetary milling for 2 h. The mass ratio of the alloy powder, AB, and PVDF was 2:4:4. The slurry was spread on a copper foil to prepare electrodes, which were dried in a vacuum chamber at room temperature for 24 h. A cell assembly was carried out under

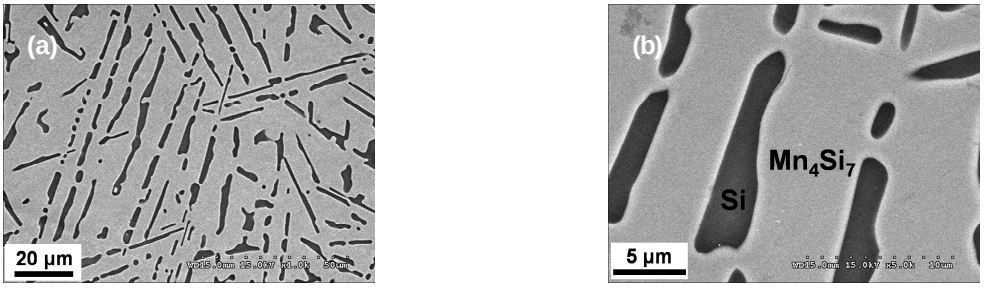

Fig. 2. SEM images of arc-melted $Si_{70}Mn_{30}$ ingots.

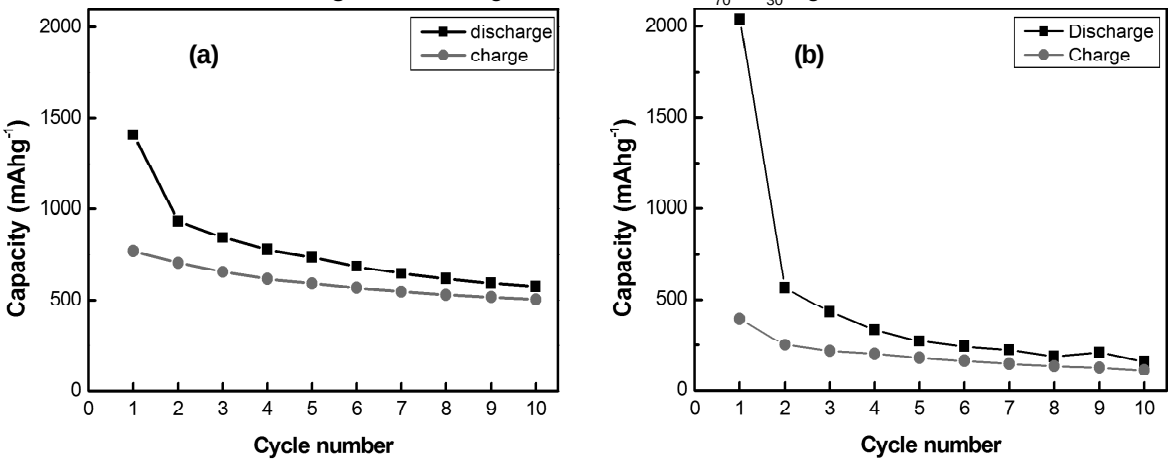

Fig. 3. Variations of the specific capacity with the cycle number of (a) melt-spun ribbons and (b) arc-melted ingots.

an argon atmosphere in a glove box, in which pure lithium was used as a counter electrode and a Celgard 2400 film as a separator. $LiPF_6$ (1 $molL^{-1}$) dissolved in EC/DEC (1:1 volume ratio) was used as the electrolyte. The electrochemical properties of the cells were measured at a 100 mAg^{-1} current density between 0.01 and 2.0 V by using a WBCS 3000 battery cycler. Microstructural evaluation and phase analysis were carried out by X-ray diffractometry (XRD), transmission electron microscopy (TEM), and scanning electron microscopy (SEM) combined with energy-dispersive spectrometry (EDS).

3. RESULTS AND DISCUSSION

3.1. Microstructures

The microstructures of the melt-spun $Si_{70}Mn_{30}$ ribbons shown in Figs. 1a and 1b represent a very fine eutectic constituent composed of silicon and a Si-Mn compound with interlamellar spacings of 110~170 nm. Fig. 1b shows an enlarged view of Fig. 1a. The EDS results obtained from areas marked "A" and "B" in Fig. 1b are shown in Figs. 1c and 1d, respectively, indicating that "A" is silicon and "B" is a Si-Mn compound. In the XRD patterns shown in Fig. 1e, two phases were identified in the melt-spun $Si_{70}Mn_{30}$ ribbons: α-Si and Mn_4Si_7. At least four Si-Mn phases have been reported to exist at compositions close to those of Mn-63at%Si: Mn_4Si_7, $Mn_{11}Si_{19}$, $Mn_{15}Si_{26}$, and $Mn_{27}Si_{47}$ [5]. The Mn_4Si_7 phase was the most probable phase to correspond to the observed diffraction peaks. This was supported by the high-resolution TEM (HRTEM) images and diffraction pattern shown in Fig. 1f. The arc-melted ingot specimen showed a relatively coarse eutectic constituent with interlamellar spacings of 6~8 μm (Fig. 2), which is approximately 40 times those observed in the melt-spun ribbons. The thickness of the silicon lamellae in the melt-spun ribbons was 50~70 nm, while that in the arc-melted specimens was 1~3 μm.

3.2. Electrochemical performance

The variations in the specific capacity of the melt-spun ribbons and the arc-melted ingots on the cycle number are shown in Fig. 3. The first discharge capacity of the melt-spun $Si_{70}Mn_{30}$ ribbons was 1408 $mAhg^{-1}$. It gradually decreased to 575 $mAhg^{-1}$ after 10 cycles. On the other hand, the first discharge capacity of the arc-melted specimen was 2041

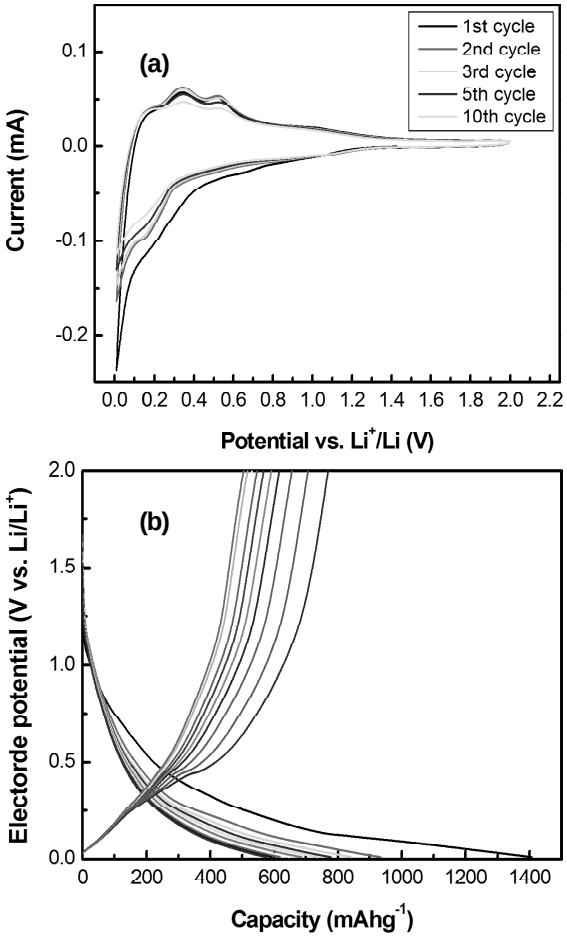

Fig. 4. Cyclic voltammograms (a) and charge/discharge curves (b) of melt-spun ribbons.

$mAhg^{-1}$, but it rapidly declined to 206 $mAhg^{-1}$ after 10 cycles. Furthermore, the initial irreversible capacity of the melt-spun ribbons was 638 $mAhg^{-1}$, while that of the arc-melted ingot specimens was 1650 $mAhg^{-1}$. These results certify an improvement in the cycle performance in the melt-spun $Si_{70}Mn_{30}$ alloy over the arc-melted specimen. The differences between the charge and discharge capacities observed at each cycle indicate that some of the inserted lithium ions were not extracted during the charge/discharge cycles.

Fig. 4 shows cyclic voltammograms (CVs) and charge/discharge curves of the melt-spun $Si_{70}Mn_{30}$ ribbons. In the first cathodic scan shown in Fig. 4a, three reduction peaks were observed at 0.6, 0.25, and 0.05 V. The first cathodic peak at 0.6 V resulted from the reductive decomposition of the electrolyte on the electrode because it disappeared in the subsequent cathodic scans, which agrees well with the results of the CVs reported by Zuo and Yin [7]. The other two peaks at 0.25 and 0.05 V declined gradually during the subsequent cycles, which were well-matched with the charge/discharge curves in Fig. 4b. In addition, the oxidation peaks occurring at 0.15, 0.3, and 0.5 V explain the charge curves in Fig. 4b. The plateau at 0.15 V was reversible, while those at 0.3 and 0.5 V almost disappeared after 10 cycles.

The improved electrochemical performance of the melt-spun $Si_{70}Mn_{30}$ ribbons is attributed to the fine microstructural scale of the active materials. As the thickness of silicon lamellae decreased 40 fold, the initial irreversible capacity was reduced by more than 2.5 times. The large initial irreversible capacity indicates that a large amount of lithium ions was not extracted probably because of the relatively long diffusion distance of the lithium ions in the arc-melted specimen. The fine silicon lamellae in the melt-spun ribbons were not seriously affected by the volume expansion/reduction during the lithium-ion insertion/extraction, unlike coarse silicon lamellae, because of the relatively large available surface area and small diffusion distance for the lithium-ion exchange. In addition, the fine and strong Mn_4Si_7 intermetallic phase appears to act as an effective inhibitor for the expansion of the silicon layer during lithium insertion.

4. CONCLUSIONS

1. The microstructure of both the $Si_{70}Mn_{30}$ melt-spun ribbons and the arc-melted ingots showed mostly a eutectic constituent composed of α-Si and a Mn_4Si_7 compound. However, the interlamellar spacings of the melt-spun ribbons were approximately 40 times smaller than those of the arc-melted ingots. As the thickness of silicon lamellae decreased 40 fold, the initial irreversible capacity was reduced by more than 2.5 times.
2. The cyclic behavior of the rapidly solidified melt-spun $Si_{70}Mn_{30}$ ribbons improved remarkably over that of the arc-melted ingots because of a finer microstructural scale. The large available surface area and small diffusion distance for the lithium-ion exchange are some of the reasons for this improvement.

ACKNOWLEDGEMENT

This work was supported by the 2007 Inje University research grant.

REFERENCES

[1] C. Menachem, E. Peled, L. Burstein and Y. Rosenberg // *J. Power Sources* **277–282** (1997) 68.

[2] T.D. Hatchard, M.N. Obrovac and J.R. Dahn // *J. Electrochem. Soc.* **152** (2005) A2335.
[3] H. Dong, X.P. Ai and H.X. Yang // *Electrochem. Commun.* **5** (2003) 952.
[4] C.S. Wang, G.T. Wu, X.B. Zhang, Z.F. Qi and W.Z. Li // *J. Electrochem. Soc.* **145** (1998) 2751.
[5] H. Li, X. Huang, L. Chen, Z. Wu and Y. Liang // *Electrochem. Solid State Lett.* **2** (1999) 547.
[6] M.D. Fleischauer, J.M. Topple and J.R. Dahn // *Electrochem. Solid-State Lett.* **8** (2005) A137.
[7] P. Zuo and G. Yin // *J. Alloys and Compounds* **414** (2006) 265-268.